Tetrahedron 73 (2017) 6386–6391

Contents lists available at ScienceDirect

Tetrahedron

journal homepage: www.elsevier.com/locate/tet

Self-recognition behavior of novel frameworks containing both urea and carboxylate anion motifs

Zhiqiang Xu [1], Haojie Ge [1], Xie Han, Sheng Hua Liu, Xiang-Gao Meng**, Jun Yin*

Key Laboratory of Pesticide and Chemical Biology, Ministry of Education, College of Chemistry, Central China Normal University, Wuhan 430079, PR China

ARTICLE INFO

Article history:
Received 24 August 2017
Received in revised form
16 September 2017
Accepted 19 September 2017
Available online 21 September 2017

Keywords:
Supramolecular
Self-recognition
Urea
Carboxylate anion
Crystal
Optical properties

ABSTRACT

Molecular recognition based on hydrogen bond interaction plays a significant role in supramolecular self-assembly. In this work, we successfully developed a class of novel frameworks containing a urea in the recognition site and a carboxylate anion in the guest unit. The self-recognition model based on the interaction between urea and carboxylate anion could induce the molecules to assemble into a highly organized form. The crystal structures showed that they assembled in highly ordered two-dimensional architectures. The optical properties showed that the position of carboxylate anion on the diphenylacetylene backbone had an obvious influence on optical properties. The self-recognition strategy is useful for the construction of highly ordered self-assembled architectures.

1. Introduction

Over recent decades, supramolecular self-assembly has developed into one of the most fascinating topics in supramolecular chemistry and a great deal of effort has been made in the design and construction of novel supramolecular architectures. These architectures assemble through many non-covalent intermolecular interactions, such as hydrogen bonding, π-π interaction, van der Waals forces, hydrophobic effect, ionic interactions and coordinative interactions.[1–12] Supramolecular self-assembly based on hydrogen bond interaction is considered to be one of the most versatile strategies for the construction of highly ordered self-assembling architectures due to many options for hydrogen bond donors and acceptors.[13–22]

Urea is a popular building block that has been widely applied in self-assembling materials.[23] The NH on the urea unit can be used as a hydrogen bond donor while the carbonyl group can play the role of hydrogen bond acceptor.

Therefore, molecules containing the urea unit can form highly ordered self-assembled structures through the intermolecular N–H···O hydrogen bond between two urea motifs, as illustrated in Fig. 1A. The hydrogen bond interaction is usually employed as the main driving force in the design of synthetic receptors for anion recognition.[24] Over past few decades, urea has been widely applied as a hydrogen bond donor in the recognition of anions.[25–29] For example, numerous studies have shown that urea can bind to acetate by forming two N–H···O hydrogen bonds in an 8-member ring, similar to the 6-member ring formed in the self-assembling process shown in Fig. 1B.[30–35]

It is possible that the interaction between urea and the carboxylate anion could also be used as an alternative model in self-assembly when the urea unit and the carboxylate anion are both installed on a molecule. Based on this self-recognition concept, we reported two novel building blocks that both contain a urea in the recognition site and a carboxylate anion in the guest unit. The crystal structures indicated that these building blocks could form two different highly ordered two-dimensional architectures. When the urea unit and carboxylate unit were located in the plane of the diphenylacetylene backbone, the molecule presented a parallel wave-shaped two-dimensional architecture with an intersection angle of 110°. When the urea unit was installed on the para-position of phenylacetylene unit and the carboxylate unit was installed on the meta-position of another phenylacetylene unit, the molecule showed a twisted wave-shaped two-dimensional

* Corresponding author.
** Corresponding author.
E-mail addresses: mengxianggao@mail.ccnu.edu.cn (X.-G. Meng), yinj@mail.ccnu.edu.cn (J. Yin).
[1] These authors contributed equally to this work.

https://doi.org/10.1016/j.tet.2017.09.036
0040-4020/

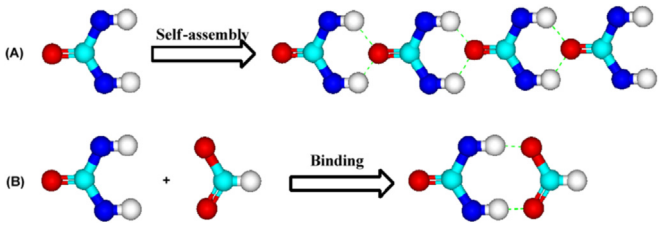

Fig. 1. The schematic representation of the self-assembly of two urea groups (A) and the binding mode between urea and acetate groups (B).

architecture with an intersection angle of ca. 124°. It was worth mentioning that the different angle between the urea-based phenylacetylene backbone and carboxylate group affected the self-assembling behavior.

2. Results and discussion

2.1. Synthesis

The synthetic route for the preparation of compounds **1a** and **1b** is outlined in Scheme 1. The deprotection of 4-((trimethylsilyl) ethynyl)aniline **2** formed intermediate **3**, according to previous literature.[36] Subsequently, the terminal alkyne **3** was subjected to the palladium-catalyzed Sonogashira coupling reaction with **4**a and **4b**,[37–39] affording respective compounds **5a** and **5b** in yields of 84–88%. Next, **5a** and **5b** were reacted with isocyanatobenzene **6** for 12 h at room temperature to form respective urea **7a** and **7b** in good yields.[40] The urea-based carboxylic acids **8a** and **8b** were obtained by the hydrolysis of **7a** and **7b** under alkaline conditions. Subsequent transformation from carboxylic acid to carboxylate anion was performed to give target molecules **1a** and **1b** in the yields of 52–54%, respectively.

All of the intermediate and target molecules were well characterized by standard spectroscopic techniques such as NMR spectroscopy and mass spectrometry.

2.2. Crystal structures of *1a* and *1b*

The solid-state structure is very significant for the investigation of the self-assembling behavior in supramolecular systems.[41,42] Great efforts were expended to obtain single crystals of compounds **1a** and **1b**. Single crystals of compounds **1a** and **1b** suitable for crystallographic analysis were grown by slow evaporation of methanol (Fig. 2). Crystal structure analysis indicates that **1a** and **1b** were crystallized in the non-centrosymmetric orthorhombic *Fdd*2 and monoclinic $P2_1/c$ space group, respectively. In both their asymmetric units, there are each one host urea derivatives anion and one counter cation N(*t*-Bu)$_4$. According to their crystal structures, the recognition of urea units and carboxylate moieties play an important role in the crystal packing.[43–45] The bond lengths and angles of **1a** and **1b** are listed, and the crystal data and structural refinements of **1a** and **1b** are summarized in Tables S1–5.

As shown in Fig. 2, due to a steric effect from the carboxylate group, the molecular conformations in **1a** and **1b** differ from each other largely. For instance, i) the central benzene ring in **1a** make two dihedral angles of 11.20(2)° and 8.97(2)° with the two neighboring phenyl groups. However, the two angles in **1b** are 23.67(2)° and 9.77(2)°, indicating an apparent molecular non-planarity in **1b**. ii) As for the often generated intermolecular $R^2_2(8)$ hydrogen-bond motif between a urea and a carboxylate group, the urea was twisted away from the carboxylate group by 9.50(2)° in **1a**. In comparison, a large angle of 42.26(2)° was resulted in **1b** due to a steric effect from the carboxylate.

In their crystal packing, the arrangement of the urea and carboxylate groups of **1a** and **1b** show that they could form well-organized, multi-dimensional architectures by using the hydrogen bonding as the driving force (Figs. 3–4). According to the crystal structure of compound **1a**, the molecules possessed two intermolecular N–H···O hydrogen bonds ($d_{N\ldots O}$ = 2.713(3) Å/ 2.896(3) Å), forming an $R^2_2(8)$ hydrogen-bonded ring and resulting in the one-dimensional chain along the [0–13] direction by glide-plane symmetry operation (Fig. 3A). Each [0–13] hydrogen-bonding chain may be connected to another by C–H···O interaction or Coulomb electrostatic interactions between the anionic and cationic ions. As for two neighboring groups of 1D chain, regular quadrilateral grids were formed between them. For compound **1b**, similar $R^2_2(8)$ hydrogen-bonded motif consisted of two intermolecular N–H···O hydrogen bonds ($d_{N2\ldots O2}$ = 2.779(2) Å and $d_{N3\ldots O3}$ = 2.847(2) Å, symmetry code: *x*, 3/2 - *y*, *z* - 1/2) could be found to mainly stabilize the [001] chain (Fig. 3B). It is worthy mentioned that the donor plane (H2/N2/C7/N3/H3) twisted away from the carboxylate plane (O2/C21/O3, 1 - *x*, 2 - *y*, - *z*) with an dihedral angle of 39.0(2)°, which should be resulted by a steric hindrance of the benzene ring.[46] Adjacent [001] chains were linked together by one

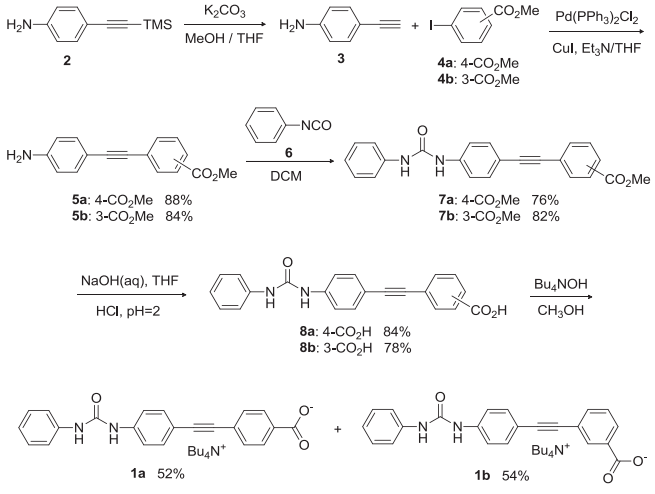

Scheme 1. Synthetic route of compounds **1a** and **1b**.

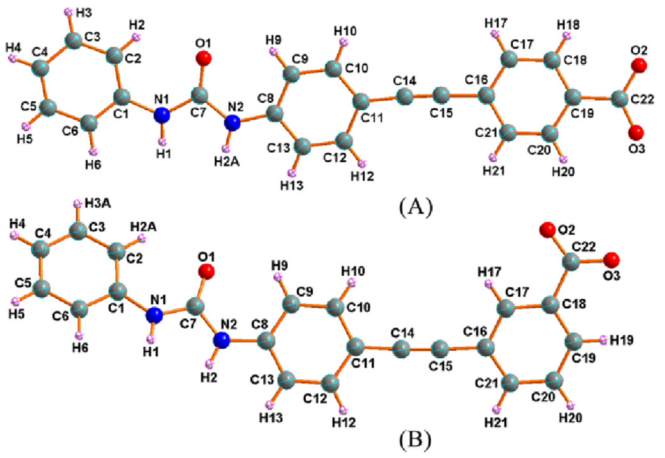

Fig. 2. Top view of the single crystal structures of **1a** (A) and **1b** (B). For clarity, the tetrabutylammonium cations were both omitted in them.

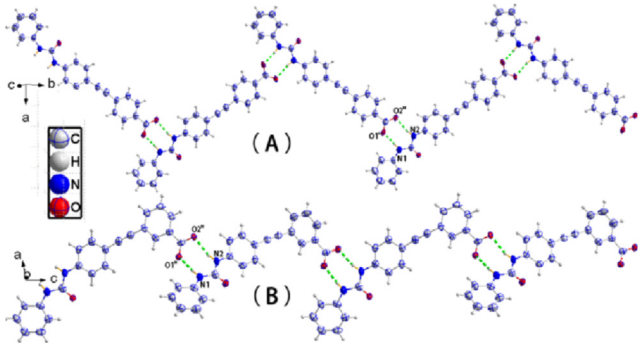

Fig. 3. One-dimensional $R^2_2(8)$ hydrogen-bonded chains in crystal packing of compounds **1a** (A) and **1b** (B). Hydrogen bonds are shown as green dashed lines. Symmetry codes: I = 1/4-*x*, *y*-1/4, 3/4 + *z*; II = *x*, 3/2-*y*, *z*-1/2. For clarity, the tetrabutyl ammonium cations were omitted.

weak C–H···O interaction ($d_{H4\ \ldots\ O2}$ = 2.505(2) Å symmetry code: 1 - *x*, 2 - *y*, - *z*), forming the 2D layer structure parallel to the (100) plane (Fig. 4B). Further analysis between these layer structures indicates one small C–H … π interaction exists between the C26 atom and acetylene π system ($d_{H26\ \ldots\ centroid}$ = 2.926(2) Å). It was worth mentioning that in crystal of **1b**, larger grid between two groups of 1D hydrogen-bonded chains were also shaped which should be ascribed to the meta-sited carboxylate group.

As for the cations in **1a** and **1b**, they are both hydrogen-bonded anchored to the carboxyl oxygen of the urea group by a non-classical intermolecular C–H···O interaction (Fig. 5) and the geometries of C–H···O hydrogen bonds for **1a** and **1b** are listed (Tables S3–4). In both the crystal structure, the N(*t*-Bu)$_4$ cations effectively inhibit a pure urea tape formation based on a six-membered hydrogen bonded ring. In one word, even the different molecular conformation and crystal packing in **1a** and **1b**, the hetero $R^2_2(8)$ hydrogen motif should be the main driving force in the molecular self-recognition.

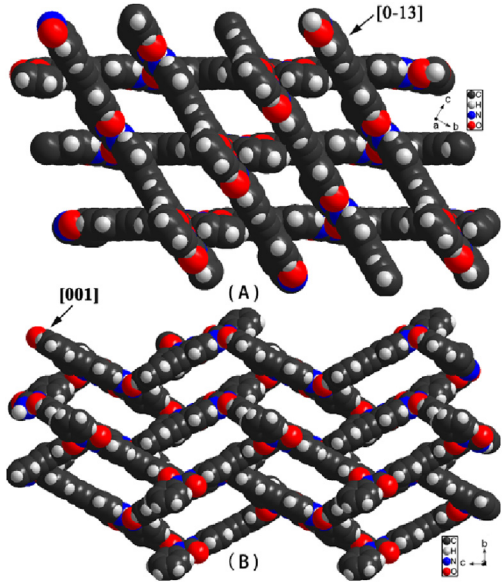

Fig. 4. Part of the crystal packing views of compound **1a** (A) and **1b** (B) showing the grid formation between two adjacent two-dimensional layer structures. For clarity, the tetrabutyl ammonium cations were omitted.

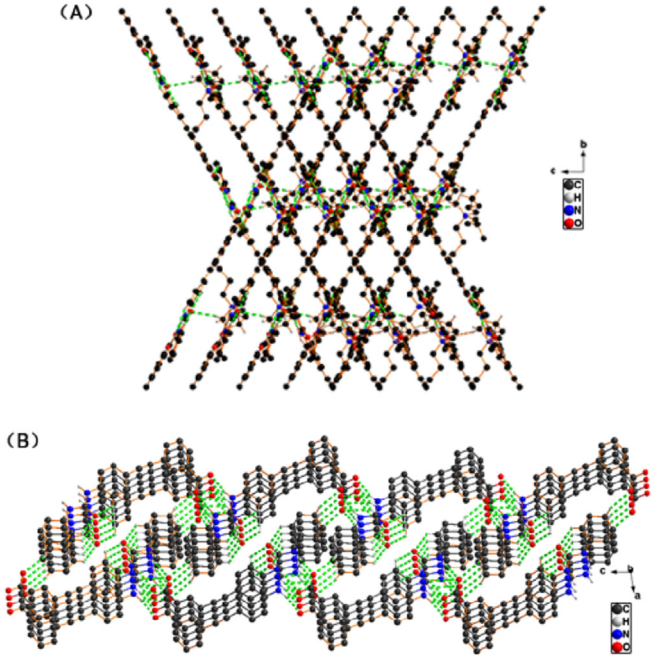

Fig. 5. The intermolecular C–H···O interaction of compound **1a** (A) and **1b** (B) (The tetrabutylammonium salts were omitted for clarity).

2.3. Optical properties of *1a* and *1b*

The optical properties of **1a** and **1b** were investigated by UV/vis absorption and fluorescence spectrometry based on our previous works.[47–54] As seen in Fig. 6, compounds **1a** and **1b** showed well-resolved absorption bands in the UV region with maximum absorption around at 310 nm in acetonitrile solution. Compared to the absorption spectra in solution, the thin film sample of **1a** revealed a broader absorption band along with a red-shift of approximately 15 nm (Fig. 6A). However, Compound **1a** showed nearly identical fluorescence spectra (350–600 nm) between solution and thin film with a maximum emission at 425 nm. In comparison to compound **1a**, the emission of compound **1b** displayed an obvious blue shift in solution and in the solid state. These results suggest that the different assembly and aggregation can affect their fluorescence manners.

Subsequently, the concentration-dependence of compounds **1a** and **1b** in UV–vis absorption and fluorescence spectrometry was investigated in acetonitrile solution. When the concentration of **1a** was increased (0.01–100 μM), the maximum absorption at 310 nm ($\varepsilon = 1.00 \times 10^4\ M^{-1}\ cm^{-1}$) distinctly increased (Fig. S3). A similar phenomenon was observed in the UV–vis absorption spectra of **1b** ($\varepsilon = 3.84 \times 10^4\ M^{-1}\ cm^{-1}$) (Fig. S4). The fluorescence emission of **1a** at 440 nm gradually increased, and the maximum emission blue-shifted to 425 nm along with an enhancement of fluorescence intensity when the concentration of **1a** was increased past 5 μM, as presented in Fig. 7A. Similarly, the fluorescence emission of **1b** at 435 nm gradually increased with increasing concentration and accompanied the blue-shift observed when the concentration of **1b** was above 1 μM (Fig. 7B). Interestingly, when the concentration of **1b** was over 30 μM, the fluorescence intensity began to decrease with increasing concentration (Fig. 7C). More probably, a higher concentration of compound **1b** led to the aggregation and the fluorescence decrease probably due to the self-bleaching or self-quenching.[55–57] These results suggested that the position of carboxylate anion on the diphenylacetylene backbone had an influence on optical properties.

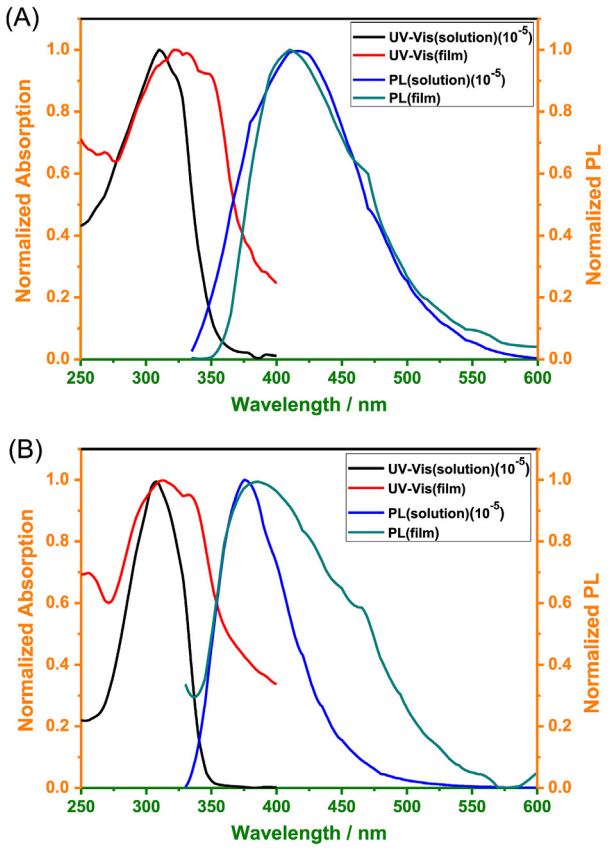

Fig. 6. Normalized UV–vis absorption and photoluminescence spectra of (A) **1a** and (B) **1b** in MeCN (10 μM) and in thin film.

2.4. Theoretical calculation

Consequently, to gain a better insight into the relationship of structure with excited state, the structures and frontier molecular orbital profiles of **1a** and **1b** were carried out by using time-dependent density functional theory (TD-DFT) calculations at the B3LYP/6-31G* level in a suite of the Gaussian 09 program. Details of the optimized structures and molecular orbital were shown in Fig. 8. Their absorption spectra and the molecular orbital containing the main electronic transitions with the largest oscillator strength have been given (Fig. 8). As shown, compound **1a** presented a planar conjugated backbone. The HOMO coefficient was nearly distributed over the whole molecule while its LUMO was predominantly located in the urea-based diphenylacetylene-carboxylate moiety. And an intense S_0–S_1 transition was predicted at around 352 nm with the largest oscillator strength of 1.8957 and contribution of 70% from HOMO to LUMO transition (Table S6 and Fig. S5). For compound **1b**, the HOMO orbital was almost assigned to the whole molecule whereas the electron density of the LUMO orbital was largely distributed over the urea-based phenylacetylene backbone, implying that it involved in an electron transfer from benzo-urea scaffold to phenylacetylene moiety as well as compound **1a**. The S_0–S_1 excitation was predicated to be the dominant transition with a maximum wavelength of 341 nm, the largest oscillator strength of 1.7828 and contribution of 70% from HOMO to LUMO (Table S6 and Fig. S5). Observations obtained from the TD-DFT implied that compounds **1a** and **1b** were fluorescent, which was well in agreement with the experimental findings. More, compound **1a** showed a narrower energy band gap (3.94 eV) in comparison to compound **1b** (4.07 eV), probably due to the effect of different position of carboxylate anion on the molecular backbone.

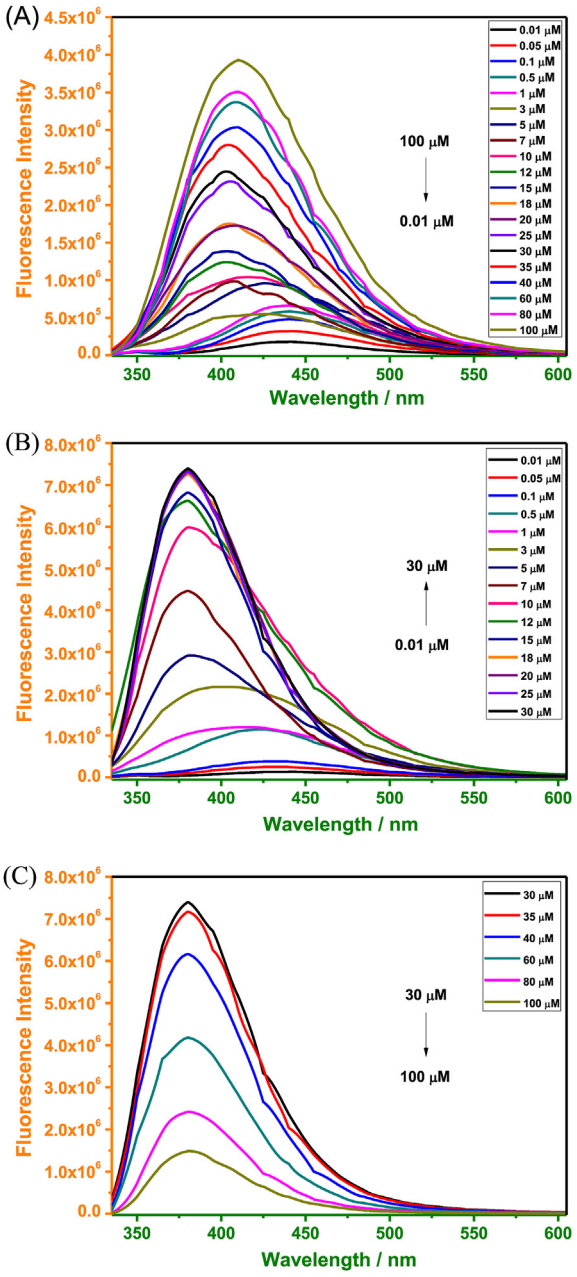

Fig. 7. The fluorescence spectra of **1a** with various concentration (0.01 μM–100 μM) (A) and **1b** with various concentration (0.01 μM–30 μM) (B) and (30 μM–100 μM) (C) in MeCN solution. (λ_{ex} = 315 nm, slit: 5/5 nm).

3. Conclusions

In summary, two novel building blocks containing both a recognition site urea and a carboxylate anion were reported, and their self-recognition behavior and optical properties were investigated. Their crystal structures showed that they could form the well-organized, two-dimensional architectures through the self-recognition driving force and their configuration were closely related to the position of the urea group and carboxylate anion on the diphenylacetylene backbone. The optical properties indicated that the position of the carboxylate anion on the diphenylacetylene backbone had an obvious influence on the optical properties and a

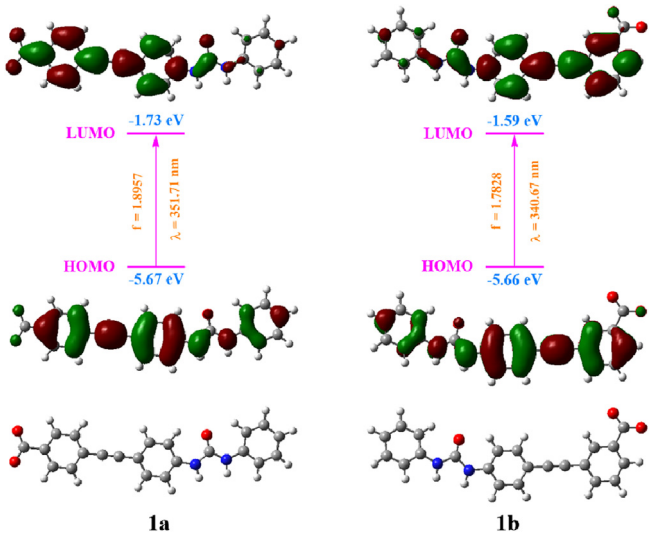

Fig. 8. Frontier molecular orbital profiles of **1a** and **1b** based on TD-DFT calculations at the B3LYP/6-31G* level by using the Gaussian 09 program.

higher concentration was required to induce the aggregation and the fluorescence decrease when the carboxylate anion was located on the meta-position of urea-based diphenylacetylene backbone. Our research provides a simple and effective strategy to construct highly ordered supramolecular architectures by through self-recognition. It is expected that this self-recognition system will be useful for the design and construction of more complicated supramolecular systems in the future.

4. Experimental

4.1. Materials and instrumentation

All manipulations were carried out under an argon atmosphere by using standard Schlenk techniques, unless otherwise stated. All commercials were used as received without further purification. ^{1}H and ^{13}C NMR spectra were collected on American Varian Mercury Plus 400 spectrometer (400 MHz) in DMSO-d_6, CD_3OD and $CDCl_3$ with tetramethylsilane (TMS) as an internal standard. The UV–vis absorption and fluorescence spectra were measured on U-3310 UV Spectrophotometer and Fluoromax-P luminescence spectrometer (HORIBA JOBIN YVON INC.), respectively. Mass spectra were measured in the EI mode or MALDI mode. The X-ray crystal-structure determinations were obtained on a Bruker APEX DUO CCD system. The theoretical calculation in the present studies were performed at the B3LYP/6-31G* level by using the Gaussian 09 program.

4.2. X-ray diffraction (XRD) crystallography

Single-Crystal of **1a** and **1b** are both too slim to be collected normally, giving their good data sets. In details, crystal **1a** was collected on a Bruker Apex (II) Duo diffractometer using *IμS*-Cu source (λ = 1.54178 Å). Crystal of **1b** was done using the graphite monochromated Mo-Ka (λ = 0.71073 Å) radiation at ambient temperature. Empirical absorption correction was applied for them. The structures were solved by direct methods and refined by the full-matrix least-squares methods on F^2 using the SHELX-97 software. All non-hydrogen atoms were refined an-isotropically. All of the hydrogen atoms were placed in the calculated positions. For **1b**, the same carbon atoms were treated as disorder. In the refinement, the commands 'DFIX' and 'ISOR' were used to constrain some related bond lengths and thermal factors.

4.3. Spectroscopic measurements

The UV–vis absorption and fluorescence spectra were measured on U-3310 UV Spectrophotometer and Fluoromax-P luminescence spectrometer (HORIBA JOBIN YVON INC.), respectively. The width of both excitation and emission slits were set at 5 nm, and the step and dwell time were set at 5.00 nm and 0.6 s, respectively.

4.4. Synthesis

4.4.1. Synthesis of *5a*

To a solution of **3** (117 mg, 1.0 mmol), methyl 4-iodobenzoate (288 mg, 1.1 mmol), $Pd(PPh_3)_2Cl_2$ (21 mg, 0.03 mmol), and CuI (5 mg, 0.03 mmol) in the mixture of THF (20 mL) and triethylamine (20 mL) was added under a nitrogen atmosphere. After being stirred at 70 °C for 6 h, the solvent was removed under reduced pressure. The residue was purified by silica gel column chromatography with dichloromethane/petroleum ether (1:2, v/v) as the eluent to afford the pure product **5a** (221 mg, 0.88 mmol) as a light brown powder in 88% yield. ^{1}H NMR (400 MHz, $CDCl_3$): δ (ppm) = 7.99 (d, J = 8.0 Hz, 2H, Ph-H), 7.54 (d, J = 8.0 Hz, 2H, Ph-H), 7.35 (d, J = 8.0 Hz, 2H, Ph-H), 6.65 (d, J = 8.0 Hz, 2H, Ph-H), 3.92 (s, 3H, CH_3), 3.87 (s, 2H, NH_2).

4.4.2. Synthesis of *5b*

The synthesis of **5b** was similar to **5a.** Light brown powder, 84% yield. ^{1}H NMR (400 MHz, $CDCl_3$): δ (ppm) = 8.17 (s, 1H, Ph-H), 7.95 (d, J = 8.0 Hz, 1H, Ph-H), 7.66 (d, J = 8.0 Hz, 1H, Ph-H), 7.40 (t, J = 8.0 Hz, 1H, Ph-H), 7.35 (d, J = 8.0 Hz, 2H, Ph-H), 6.65 (d, J = 8.0 Hz, 2H, Ph-H), 3.93 (s, 3H, CH_3), 3.85 (s, 2H, NH_2). ^{13}C NMR (100 MHz, $CDCl_3$): δ (ppm) = 166.1, 146.4, 135.0, 132.6, 132.0, 129.8, 128.1, 128.0, 123.9, 114.3, 111.6, 90.7, 85.9, 51.8. MS (EI) m/z: calcd for $C_{16}H_{13}NO_2$ 251.09, found 251.24.

4.4.3. Synthesis of *7a*

To a solution of **5a** (251 mg, 1.0 mmol), isocyanatobenzene (142 mg, 1.2 mmol) in dry DCM (50 mL) was added under a nitrogen atmosphere. After the resulting solution was heated to reflux and stirred for 12 h, the solvent was removed under reduced pressure. The residue was purified by silica gel column chromatography with dichloromethane/petroleum ether (3:1, v/v) as the eluent to afford the pure compound **7a** (111 mg, 0.3 mmol) as a white crystalline solid in 76% yield. ^{1}H NMR (400 MHz, DMSO-d_6): δ (ppm) = 9.01 (s, 1H, NH), 8.81 (s, 1H, NH), 7.98 (d, J = 8.0 Hz, 2H, Ph-H), 7.66 (d, J = 8.0 Hz, 2H, Ph-H), 7.58–7.49 (m, 4H, Ph-H), 7.46 (d, J = 8.0 Hz, 2H, Ph-H), 7.29 (t, J = 8.0 Hz, 2H, Ph-H), 6.99 (t, J = 8.0 Hz, 1H, Ph-H), 3.87 (s, 3H, CH_3). ^{13}C NMR (100 MHz, DMSO-d_6) δ (ppm) = 170.8, 157.4, 146.0, 144.5, 137.6, 136.5, 134.5, 133.9, 132.6, 127.6, 123.4, 123.1, 119.5, 98.1, 92.6, 57.4. MS (EI) m/z: calcd for $C_{23}H_{18}N_2O_3$ 370.13, found 370.40.

4.4.4. Synthesis of *7b*

The synthesis of **7b** was similar to **7a.** White solid, 82% yield. ^{1}H NMR (400 MHz, DMSO-d_6): δ (ppm) = 8.92 (s, 1H, NH), 8.75 (s, 1H, NH), 8.04 (s, 1H, Ph-H), 7.95 (d, J = 8.0 Hz, 1H, Ph-H), 7.80 (d, J = 8.0 Hz, 1H, Ph-H), 7.59 (d, J = 8.0 Hz, 1H, Ph-H), 7.52 (s, 4H, Ph-H), 7.46 (d, J = 8.0 Hz, 2H, Ph-H), 7.30 (t, J = 8.0 Hz, 2H, Ph-H), 6.98 (t, J = 8.0 Hz, 1H, Ph-H), 3.88 (s, 3H, CH_3). ^{13}C NMR (100 MHz, DMSO-d_6): δ (ppm) = 168.1, 154.9, 143.3, 142.1, 138.1, 135.0, 134.2, 132.8, 132.0, 131.4, 126.0, 124.7, 121.0, 120.6, 117.2, 93.5, 89.7, 55.0. MS (EI) m/z: calcd for $C_{23}H_{18}N_2O_3$ 370.13, found 370.37.

4.4.5. Synthesis of **8a**

To a solution of **7a** (111 mg, 0.3 mmol) in THF (20 mL) was added 1 M NaOH aqueous solution (15 mL) under a nitrogen atmosphere. After the resulting solution was stirred at 60 °C for 12 h, the reaction mixture was cooled to room temperature. Then the solution was acidified to a pH of 2 using 6 M HCl and extracted with ethyl acetate (4 × 80 mL). The organic layer was washed with H_2O (30 mL), dried with anhydrous sodium sulfate and concentrated in vacuum. The residue was recrystallized from DCM/hexane to afford the pure product **8a** (90 mg, 0.25 mmol) as a light brown powder in 84% yield. ^{1}H NMR (400 MHz, DMSO-d_6): δ (ppm) = 10.51 (s, 1H), 10.30 (s, 1H), 9.14 (s, 1H), 7.98 (d, J = 8.0 Hz, 2H, Ph-H), 7.65 (d, J = 8.0 Hz, 2H, Ph-H), 7.51–7.61 (m, 4H, Ph-H), 7.48 (d, J = 8.0 Hz, 2H, Ph-H), 7.27 (t, J = 8.0 Hz, 2H, Ph-H), 6.95 (t, J = 8.0 Hz, 1H, Ph-H). ^{13}C NMR (100 MHz, CD_3SOCD_3): δ (ppm) = 171.5, 157.1, 145.7, 144.3, 137.3, 136.2, 135.1, 134.5, 133.7, 133.0, 127.0, 122.3, 123.0, 119.5, 97.7, 92.7. MS (EI) m/z: calcd for $C_{22}H_{16}N_2O_3$ 356.12, found 356.61.

4.4.6. Synthesis of **8b**

The synthesis of **8b** was similar to **8a.** Light brown powder, 78% yield. ^{1}H NMR (400 MHz, CD_3SOCD_3): δ 8.93 (s, 1H, NH), 8.76 (s, 1H, NH), 8.03 (s, 1H, Ph-H), 7.94 (d, J = 8.0 Hz, 1H, Ph-H), 7.77 (d, J = 8.0 Hz, 1H, Ph-H), 7.55 (t, J = 4.0 Hz, 1H, Ph-H), 7.48–7.54 (m, 4H, Ph-H), 7.46 (d, J = 8.0 Hz, 2H, Ph-H), 7.29 (t, J = 8.0 Hz, 2H, Ph-H), 6.99 (t, J = 8.0 Hz, 1H, Ph-H). ^{13}C NMR (100 MHz, CD_3SOCD_3): δ (ppm) = 169.3, 154.9, 143.2, 142.1, 137.8, 135.0, 134.4, 134.0, 131.8, 131.7, 131.5, 125.8, 124.7, 121.0, 120.6, 117.3, 93.3, 89.9. MS (EI) m/z: calcd for $C_{22}H_{16}N_2O_3$ 356.12, found 356.36.

4.4.7. Synthesis of **1a**

To a solution of **8a** (53 mg, 0.15 mmol) in dry methanol (20 mL) was added a solution of 0.8 M Bu_4NOH (0.50 mL, 0.40 mmol) in dry methanol (40 mL) dropwise over 2 h. After the resulting solution was stirred at room temperature for 12 h, the solvent was removed under reduced pressure. The residue was recrystallized from DCM to afford the pure product **1a** (47 mg, 0.08 mmol) as a light brown powder in 52% yield. ^{1}H NMR (400 MHz, CD_3OD): δ (ppm) = 7.85 (d, J = 8.0 Hz, 2H, NH), 7.45–7.38 (m, 6H, Ph-H), 7.35 (d, J = 8.0 Hz, 2H, Ph-H), 7.21 (t, J = 8.0 Hz, 2H, Ph-H), 6.94 (t, J = 8.0 Hz, 1H, Ph-H), 3.10–3.19 (m, 8H, N–CH_2), 1.57 (dt, J = 16.0, 8.0 Hz, 8H, CH_2), 1.33 (dd, J = 16.0, 8.0 Hz, 8H, CH_2), 0.94 (t, J = 8.0 Hz, 12H, CH_3). The solubility of 1a was not good, so it was hard to get its ^{13}C NMR. MALDI-TOF: MS m/z 357.20 [M - Bu_4N^+ + $2H^+$]$^+$; calcd exact mass 597.39.

4.4.8. Synthesis of **1b**

The synthesis of **1b** was similar to **1a.** Light brown powder, 54% yield. ^{1}H NMR (400 MHz, CD_3OD): δ (ppm) = 8.06 (s, 1H, NH), 7.90 (d, J = 8.0 Hz, 1H, NH), 7.52 (d, J = 8.0 Hz, 1H, Ph-H), 7.45–7.50 (m, 4H, Ph-H), 7.43 (d, J = 8.0 Hz, 2H, Ph-H), 7.35 (t, J = 8.0 Hz, 1H, Ph-H), 7.28 (t, J = 8.0 Hz, 2H, Ph-H), 7.02 (t, J = 4.0 Hz, 1H, Ph-H), 3.18–3.25 (m, 8H, N–CH_2), 1.64 (dd, J = 16.0, 8.0 Hz, 8H, CH_2), 1.40 (dd, J = 16.0, 8.0 Hz, 8H, CH_2), 1.01 (t, J = 8.0 Hz, 12H, CH_3). The solubility of **1b** was not good, so it was hard to get its ^{13}C NMR. MALDI-TOF: MS m/z 357.19 [M - Bu_4N^+ + $2H^+$]$^+$; calcd exact mass 597.39.

Acknowledgements

The authors acknowledge financial support from National Natural Science Foundation of China (21676113, 21402057, 21472059); Youth Chen-Guang Project of Wuhan (2016070204010098). Supported by the 111 Project B17019 and the Ministry-Province Jointly Constructed Base for State Key Lab-Shenzhen Key Laboratory of Chemical Biology, Shenzhen; Supported by self-determined research funds of CCNU from the colleges' basic research and operation of MOE (CCNU16A02004).

Appendix A. Supplementary data

Supplementary data related to this article can be found at https://doi.org/10.1016/j.tet.2017.09.036.

References

1. Würthner F, Saha-Möller CR, Fimmel B, Ogi S, Leowanawat P, Schmidt D. *Chem Rev*. 2016;116:962–1052.
2. Dale EJ, Vermeulen NA, Juríček M, et al. *Acc Chem Res*. 2016;49:262–273.
3. Erbas-Cakmak L, Leigh DA, McTernan CT, Nussbaumer AL. *Chem Rev*. 2015;115, 10081–10206.
4. Xue M, Yang Y, Chi X, Yan X, Huang F. *Chem Rev*. 2015;115, 7398–7501.
5. Gilday LC, Robinson SW, Barendt TA, Langton MJ, Mullaney BR, Beer PD. *Chem Rev*. 2015;115:7118–7195.
6. Yu G, Jie K, Huang F. *Chem Rev*. 2015;115:7240–7303.
7. Han Y, Meng Z, Ma YX, Chen CF. *Acc Chem Res*. 2014;47:2026–2040.
8. Hu XY, Xiao T, Lin C, Huang F, Wang L. *Acc Chem Res*. 2014;47:2041–2051.
9. Guo DS, Liu Y. *Acc Chem Res*. 2014;47:1925–1934.
10. Shimizu LS, Salpage SR, Korous AA. *Acc Chem Res*. 2014;47:2116–2127.
11. Zhang DW, Zhao X, Hou JL, Li ZT. *Chem Rev*. 2012;112:5271–5316.
12. De Greef TFA, Smulders MMJ, Wolffs M, Schenning AP, Sijbesma RP, Meijer EW. *Chem Rev*. 2009;109:5687–5754.
13. Huo Y, Zeng H. *Acc Chem Res*. 2016;49:922–930.
14. Han X, Hu F, Ge H, Liu SH, Yin J. *Prog Chem*. 2015;27:675–686.
15. Busschaert N, Caltagirone C, Rossom WV, Gale PA. *Chem Rev*. 2015;115, 8038–8155.
16. Shimizu LS, Salpage SR, Korous AA. *Acc Chem Res*. 2014;47:2116–2127.
17. Seki T, Lin X, Yagai S. *Asian J Org Chem*. 2013;2:708–724.
18. G1owacki ED, Irimia-Vladu M, Bauer S, Sariciftci NS. *J Mater Chem B*. 2013;1: 3742–3753.
19. Lee S, Flood AH. *J Phys Org Chem*. 2013;26:79–86.
20. Zhao X, Li ZT. *Chem Commun*. 2010;46:1601–1616.
21. Yan X, Jiang B, Cook TR, et al. *J Am Chem Soc*. 2013;135:16813–16816.
22. Ji X, Shi B, Wang H, et al. *Adv Mater*. 2015;27:8062–8066.
23. Custelcean R. *Chem Commun*. 2008:295–307.
24. Hu F, Cao M, Huang J, et al. *Dyes Pigm*. 2015;119:108–115.
25. Jia C, Zuo W, Zhang D, Yang XJ, Wu B. *Chem Commun*. 2016;52:9614–9627.
26. Custelcean R. *Chem Commun*. 2013;49:2173–2182.
27. Dydio P, Lichosyt D, Jurczak J. *Chem Soc Rev*. 2011;40:2971–2985.
28. Amendola V, Fabbrizzi L, Mosca L. *Chem Soc Rev*. 2010;39:3889–3915.
29. Li AF, Wang JH, Wang F, Jiang YB. *Chem Soc Rev*. 2010;39:3729–3745.
30. Bose P, Dutta R, Ghosh P. *Org Biomol Chem*. 2013;11:4581–4584.
31. Moore SJ, Haynes CJE, González J, et al. *Chem Sci*. 2013;4:103–117.
32. Gale PA, Hiscock JR, Lalaoui N, Light ME, Wells NJ, Wenzel M. *Org Biomol Chem*. 2012;10:5909–5915.
33. Jiménez MB, Alcázar V, Peláez R, Sanz F, Fuentes de Arriba ÁL, Caballero MC. *Org Biomol Chem*. 2012;10:1181–1185.
34. Bergamaschi G, Boiocchi M, Monzani E, Amendola V. *Org Biomol Chem*. 2011;9: 8276–8283.
35. Dial BE, Rasberry RD, Bullock BN, Smith MD, Pellechia Jr PJ, Shimizu KD. *Org Lett*. 2011;13:244–247.
36. Marqués-González S, Yufit DS, Howard JA, et al. *Dalton Trans*. 2013;42: 338–341.
37. Ou YP, Jiang C, Wu D, et al. *Organometallics*. 2011;30:5763–5770.
38. Wu D, Zhang H, Liang J, et al. *J Org Chem*. 2012;77:11319–11324.
39. Phetrak N, Rukkijakan T, Sirijaraensre J, et al. *J Org Chem*. 2013;78: 12703–12709.
40. Li Z, Zhang C, Ren Y, Yin J, Liu SH. *Org Lett*. 2011;13:6022–6025.
41. Seth SK, Sarkar D, Roy A, Kar T. *CrystEngComm*. 2011;13:6728–6741.
42. Moulton B, Zaworotko MJ. *Chem Rev*. 2001;101:1629–1658.
43. Brooks SJ, Gale PA, Light ME. *CrystEngComm*. 2005;7:586–591.
44. Wang J, Li S, Yang P, Huang X, Yang XJ, Wu B. *CrystEngComm*. 2013;15: 4540–4548.
45. Basu A, Das G. *J Org Chem*. 2014;79:2647–2656.
46. Zafar A, Geib SJ, Hamuro Y, Hamilton AD. *New J Chem*. 1998;137:137–141.
47. Cao M, Chen H, Chen D, et al. *Chem Commun*. 2016;52:721–724.
48. Wu D, Chen Z, Zhang Y, Zhang J, Liu SH, Yin J. *J Org Chem*. 2015;80:8443–8448.
49. Wu D, Zhang Y, Zhang J, Liu SH, Yin J. *Chem Asian J*. 2015;10:1344–1353.
50. Wu D, Zhang H, Liu SH, Yin J. *Chem Asian J*. 2015;10:602–607.
51. Wu D, Ge H, Chen Z, et al. *Org Biomol Chem*. 2014;12:8902–8910.
52. Huang J, Wu D, Ge H, Liu SH, Yin J. *Chin Chem Lett*. 2014;25:1399–1402.
53. Wu D, Ge H, Liu SH, Yin J. *RSC Adv*. 2013;3:22727–22738.
54. Zhang H, Wu D, Liu SH, Yin J. *Curr Org Chem*. 2012;16:2124–2158.
55. He W, Zhang L, Han B, et al. *J Mater Chem B*. 2013;1:3257–3266.
56. Petrou PS, Mastichiadis C, Christofidis I, Kakabakos SE. *Anal Chem*. 2007;79: 647–653.
57. Chen WY, Young LJ, Lu M, et al. *Nano Lett*. 2017;17:143–149.